ACS APPLIED MATERIALS & INTERFACES

Research Article

www.acsami.org

Facile Hydrothermal Synthesis of VS_2/Graphene Nanocomposites with Superior High-Rate Capability as Lithium-Ion Battery Cathodes

Wenying Fang,[†] Hongbin Zhao,*[,†,‡] Yanping Xie,[†] Jianhui Fang,[†] Jiaqiang Xu,[†] and Zhongwei Chen*[,‡]

[†]Department of Chemistry, College of Science, Shanghai University, No. 99 Shangda Road, Shanghai 200444, People's Republic of China

[‡]Department of Chemical Engineering, University of Waterloo, 200 University Ave. West, Waterloo N2L 3G1, Canada

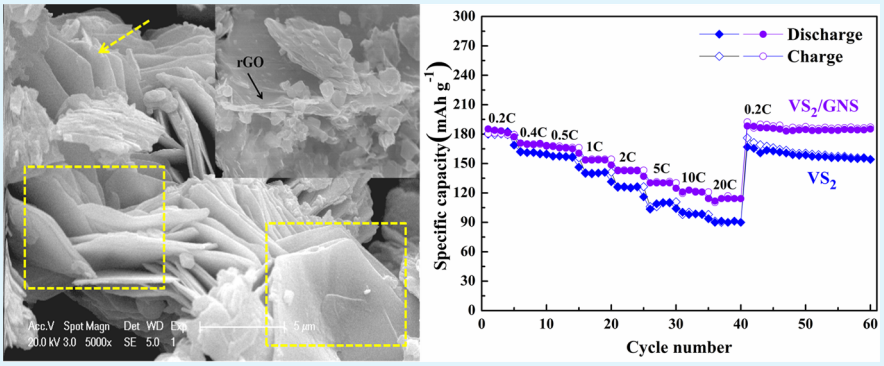

ABSTRACT: In this study, a facile one-pot process for the synthesis of hierarchical VS_2/graphene nanosheets (VS_2/GNS) composites based on the coincident interaction of VS_2 and reduced graphene oxide (rGO) sheets in the presence of cetyltrimethylammonium bromide is developed for the first time. The nanocomposites possess a hierarchical structure of 50 nm VS_2 sheets in thickness homogeneously anchored on graphene. The VS_2/GNS nanocomposites exhibit an impressive high-rate capability and good cyclic stability as a cathode material for Li-ion batteries, which retain 89.3% of the initial capacity 180.1 mAh g^{-1} after 200 cycles at 0.2 C. Even at 20 C, the composites still deliver a high capacity of 114.2 mAh g^{-1} corresponding to 62% of the low-rate capacity. Expanded studies show that VS_2/GNS, as an anode material, also has a good reversible performance with 528 mAh g^{-1} capacity after 100 cycles at 200 mA g^{-1}. The excellent electrochemical performance of the composites for reversible Li^+ storage should be attributed to the exceptional interaction between VS_2 and GNS that enabled fast electron transport between graphene and VS_2, facile Li-ion diffusion within the electrode. Moreover, GNS provides a topological and structural template for the nucleation and growth of two-dimensional VS_2 nanosheets and acted as buffer matrix to relieve the volume expansion/contraction of VS_2 during the electrochemical charge/discharge, facilitating improved cycling stability. The VS_2/GNS composites may be promising electrode materials for the next generation of rechargeable lithium ion batteries.

KEYWORDS: *graphene, transition metal dichalcogenides, layered-VS_2, cathode materials, lithium ion batteries*

INTRODUCTION

In addition to the still-existing serious environmental problems such as greenhouse effect and acid rain, the new exposing haze caused by harmful fine-particulate-matter (PM 2.5) in the atmosphere from combustion of fossil fuels and gas emission of automobiles are serious problems humankind are facing. Undoubtedly, there is an urgent need to develop alternative clean and sustainable energy technologies to initiate large scale applications of wind energy, solar energy, and zero-emission electric vehicles (EVs) or low emission hybrid electric vehicles (HEVs) to alleviate the increasingly serious air pollution.[1] Lithium ion batteries (LIBs) have been widely considered as one of the leading and promising candidates for electric vehicles and energy storage.[2,3] Naturally, it is important to realize the requirements of designing reliable electrode materials with flexible properties and high electrochemical performances in the aspect of high energy and power density, long lifespan, low self-discharge rate, and so on. Therefore, various electrochemically active materials have been recently reported and investigated for lithium ion storage.[4−6]

Since the spectacular and groundbreaking discovery of monolayer graphene with excellent physical and chemical performance,[7,8] two-dimensional (2D) transition metal layered materials have been remarkably concentrated as a technological research focus. Because of their unique and neoteric physical properties attributed to the layered structure, the presence of d-electrons of transition metals, and the high specific surface areas, 2D transition metal layered materials are important for sensing, catalysis, and energy storage applications.[9,10] Particularly, besides graphene, other 2D compounds such as ZnO,

Received: April 14, 2015
Accepted: May 28, 2015
Published: May 28, 2015

DOI: 10.1021/acsami.5b03124
ACS Appl. Mater. Interfaces 2015, 7, 13044−13052

transition metal oxides, and transition metal dichalcogenides (TMDs) are of remarkable interest due to their unique properties that are useful for applications including a new generation of field effect transistors, photo emitting devices, hydrogen storage, energy conversion, and storage devices.[10−14] Among these materials, layered transition metal dichalcogenides (LTMDs), such as MoS_2, VS_2, WS_2, FeS_2, CoS_2, and NiS_2, have attracted increasing interest as graphene analogues because of their unique properties and applications to electronics, energy storage, and so on.[15−20] LTMDs are versatile intercalation hosts that can adapt the stereoscopic demands of a wide class of guest species. Their ability to form intercalation compounds is strongly dependent on the electronic structure of the dichalcogenide. 2D layered VS_2, which have been found to be a typical member of the LTMDs family, have been confirmed that the structure can exist both in 2H and 1T-phase with V sandwiched between two S layers and the S−V−S trilayers, which forms a stacked unit via weak van der Waals force.[21] This unique structure can intrinsically accommodate guest ions to insert the interlayer spacing without a serious structural distortion and allow for their fast transport during charging and discharging cycles. Moreover, LTMDs have a larger interlayer spacing than graphite, and offer a wide range of electron affinity and sufficient space for the intercalation of guest ions.[22] Additionally, 2D layered nanomaterials showed excellent electric conduction, high aspect ratios, ultrathin edges, and good mechanical properties.[14,23] Therefore, VS_2 was predicted to be widely used as a layered potential material for its moisture responsiveness, efficient field emission properties, catalytic characteristics, and high two-dimension conductive abilities.[24−28] Moreover, with excellent electrical conductivity, unique electrical structure, and high specific surface area, layered VS_2 satisfies the requirements as a basis for developing a promising candidate electrode material for LIBs.[29,30]

As previously reported, graphene is believed to be one of the most desirable carbon matrices in solvothermal systems for improving electrochemical performances of active materials distributed on the surface of graphene or between the graphene nanosheets due to the high electric conductivity, large specific surface area, good flexibility, and high stability, as well as a unique structure.[31−34] Apparently, the hybrid system intriguingly exhibits a high electrochemical performance due to the graphene that plays a key role in the rapid electron transport and effective buffering of the volume expansion. Graphene can be regarded as a "binder" to prevent the separation of the bulk active materials from the current collector in the case of localized pulverization. Nethravathi et al. reported a facile hydrothermal reaction for yielding graphene and a nanotubular metastable monoclinic polymorph of VO_2,[35] and N-doped graphene-VO_2 nanosheet-built 3D flower hybrid,[36] which both showed potential to be high capacity and cycle stability cathode materials for LIBs. Zhao and co-workers[37] reported a surfactant-assisted chemical reaction-deposition method to synthesize a hybrid material of sulfur encapsulated in reduced graphene oxide (rGO) sheets for rechargeable lithium batteries that exhibited a high specific capacity, enhanced rate capability, excellent cyclic stability, and effectively alleviated the shuttle phenomenon of polysulfides in organic electrolyte as a result of the presence of rGO.

Herein, we report a facile one-step hydrothermal synthesis of VS_2/graphene nanosheets (VS_2/GNS) based on the coincident interaction of VS_2 and rGO using cetyltrimethylammonium bromide (CTAB) as a template without further heat treatment. It demonstrates that the VS_2/GNS hybrids show promising signs as a potential 2D material to be utilized in energy storage devices, in particular, as a Lithium ion storage material, owing to its high capacity, good cyclic stability and excellent rate capability, which are superior to VS_2 alone. Benefiting from the unique hierarchical architecture, the hybrids are expected to play an important role of being used as a cathode material for LIBs.

EXPERIMENTAL SECTION

Synthesis of VS_2/GNS Composites. All purchased chemicals were analytical grade and used without further purification. The in situ synthesis of VS_2/GNS composites is shown schematically in Figure 1.

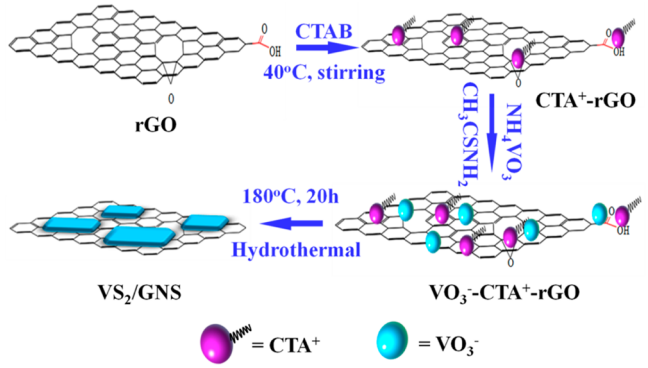

Figure 1. Schematic illustration for the in situ synthesis of VS_2/GNS by a CTAB-assisted method.

Graphene oxide (GO) was prepared from natural graphite powder by a modified Hummers method.[38] The as-prepared GO was dried under 80 °C for 24 h following a sharp thermal swelling in a 1000 °C quartz tube for 30 s accompanied by large quantity argon (Ar) airflow, then moved to another 400 °C quartz tube for 5 min under the same airflow before cooling naturally to the ambient environment. The obtained reduced graphene oxide (rGO) was supersonically redispersed in a mixed solution of 30 mL deionized water and 6 mL ammonia after grinding in a agate mortar. Then, suitable quality CTAB was added to the former suspension to form a homogeneous mixture with continuous stirring at 40 °C in a water bath for 24 h to allow CTA^+ to adsorb onto the GNS surface by electrostatic interaction.[39] Then, 4 mmol ammoniumvanadate (NH_4VO_3) was introduced to the established solution still under vigorous stirring until the NH_4VO_3 was completely dissolved. After that, 20 mmol thioacetamide (CH_3CSNH_2) was added to the above solution under magnetic stirring. The final solution was transferred into a Teflon-lined stainless-steel autoclave with a capacity of 50 mL, which was sealed after eliminating the air with Ar for several minutes and kept at 180 °C for 20 h. After cooling naturally to room temperature, the black product was collected by filtration and washed with ethanol and distilled water, followed by drying at 80 °C for 12 h under vacuum. The obtained black powder is called VS_2/GNS. For comparison, VS_2 and corresponding materials was prepared following the same procedure.

Materials Characterization. The X-ray diffraction (XRD) patterns of the samples were recorded on a Rigaku D/max 2200 X-ray diffractometer with Cu Ka radiation (λ = 1.54056 Å). Morphology analysis was performed with a JEOL JSM-6700F scanning electron microscope (SEM). High-resolution transmission electron microscopy (HRTEM) images were characterized with a JEOL JEM−200CX microscope operating at 200 kV. The carbon content in the VS_2/GNS composite is about 3.9 wt %, which was analyzed via Vario EL-III elemental analyzer (Elementar, Germany). FT-IR spectrum was obtained by an infrared spectrometer (Shimadzu, UV-2501PC, Japan). More detailed structural information on the composites were

DOI: 10.1021/acsami.5b03124
ACS Appl. Mater. Interfaces 2015, 7, 13044−13052

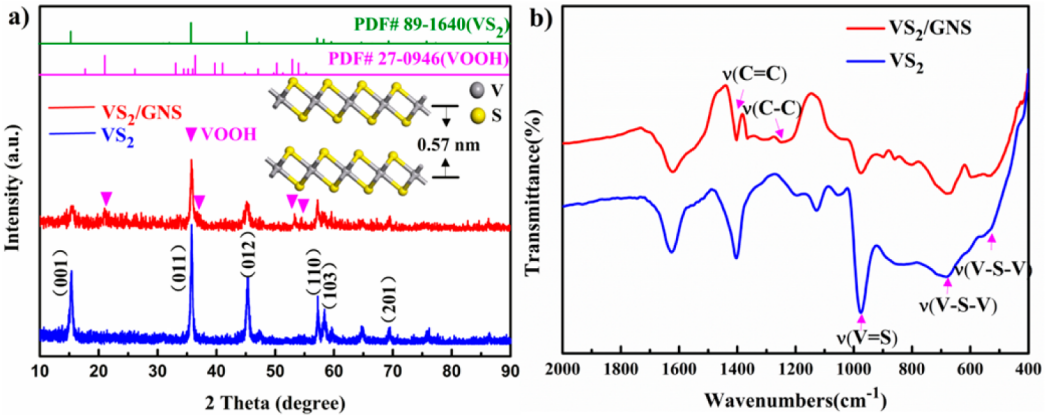

Figure 2. (a) XRD patterns of VS_2 and VS_2/GNS; (inset) side-view atomic structures of VS_2. (b) FTIR spectra of VS_2 and VS_2/ GNS.

obtained by a laser Raman spectrometer (Renishaw inVia plus) with a laser wavelength of 633 nm.

Electrochemical Measurements. Two-electrode test cells were used for the electrochemical measurements. The working electrode was fabricated by casting a slurry of 70 wt % active material, 20 wt % conductive agent (acetylene black), and 10 wt % binder (polyvinylidene fluoride) in *N*-methyl-2-pyrrolidinone (NMP) on a aluminum (cathode) or copper (anode) foil, dried at 80 °C in vacuum for 12 h, and then compressed. The test cells were assembled in an argon-filled glovebox, using a lithium sheet as the counter and reference electrode, a microporous membrane (Celgard 2400) separator, and an electrolyte of 1.0 M $LiPF_6$ solution in a 1:1 (v/v) mixture of ethylene carbonate and dimethyl carbonate. Galvanostatic charging and discharging was performed on a CT2001A Land Battery Testing System. All the specific capacities were calculated merely based on the mass of VS_2. Cyclic voltammetry (CV) at a sweep rate of 0.1 mV s^{-1} was performed on an electrochemical workstation (CHI 660D). Specifically, electrochemical impedance spectroscopy (EIS) was carried out on a Solartron 1287 electrochemical interface +1255B frequency analyzer by applying a sine wave with an amplitude of 5 mV in the frequency range 100 kHz to 0.01 Hz. All electrochemical measurements were carried out at room temperature.

RESULTS AND DISCUSSION

In this work, we designed a hybrid VS_2/GNS composite by CTAB-assisted hydrothermal method and demonstrated its electrochemical performances stemming from the unique sheet-like morphology, which benefits lithium ion diffusion and fast charge transfer. As shown in Figure 1, CTAB, as a linker between the precursor of vanadium oxides and graphene,[40] was employed to control the growth of VS_2 on the surface of graphene. To be specific, the adsorption of CTA^+ on the rGO surface formed the positively charged rGO, which assisted in overcoming the charge repulsion between rGO and VO_3^-. Graphene nanosheets with superior properties such as outstanding electronic behavior, large surface area, and amazing mechanical properties in the field of batteries, can act as ideal substrates for the nucleation and subsequent growth of XS_2.[41−43] Consequently, an ideal structure is fabricated through hydrothermal reduction of rGO and VO_3^- to VS_2/GNS composites. In this process, synergistic interaction of CTAB and graphene is supposed to facilitate synthesis of the target composites, and graphene in the hybrids may provide better cushion for the volume expension for reversible Li^+ insertion/extraction than pristine VS_2.

The structure and morphology of VS_2 and VS_2/GNS composites prepared by the CTAB-assisted process were analyzed in details. The XRD patterns of as-prepared VS_2 and VS_2/GNS composites in Figure 2a can readily be indexed to be hexagonal VS_2 (JCPDS 89-1640) with a space group of $P\bar{3}m1$. The typical layered VS_2 diffraction peaks at 15.4, 35.7, 44.2, 57.2, 58.3, and 69.3° are clearly observed and correspond to the (001), (011), (012), (110), (103), and (201) lattice planes, respectively. The characteristic (001) diffraction at 15.2°, corresponding to an interlayer *d*-spacing of 0.567 nm, indicates a stacked lamellar structure. In other words, both of the XRD patterns of VS_2 and VS_2/GNS composites in Figure 2a show the special VS_2 (001) reflection, which is the distinctive and significant peak for researching the structure of layered VS_2. Also, the stacking ordered degree of VS_2/GNS along the *c*-axis direction can be judged from the peak intensity. Obviously, the XRD patterns of VS_2/GNS composites show that the stacking of the (001) plane was inhibited from the weakened peak intensity as compared to pure VS_2 due to the presence of rGO, and the intensity of the other lower reflection peaks were reduced as well.[24,25,44] It is worthy to note that the (001) lattice plane, which presents to be related with a typical layered structure, is weaker than (011), indicating a separation of VS_2 nanosheets and competitive orientation between these two different planes.[45] The other diffraction peaks of VS_2/GNS are in accordance with the electron diffraction pattern in Figure 2a, except for four weak reflections located at 21.1, 36.54, 53.1, and 54.1°, which are the characteristic peaks from (110), (111), (221), and (240) planes of the orthorhombic-phase VOOH (JCPDS 27-0946) mainly caused by the side reaction.[46] Furthermore, we can hardly detect the (002) diffraction peaks of graphene at 26.2° in the XRD patterns of the hybrids, indicating that the only 3.9 wt % theoretical content of ultrathin rGO in this composites seldom stacks during hydrothermal process.[41,47]

A further FT-IR spectrum comparison of the VS_2/GNS with that of pure VS_2 confirms the presence of V^{4+} oxidation state in the composites (Figure 2b). There is no significant change in the features of both V═S and V−S−V peaks, which could be attributed to the great number of V^{4+} centers present in the nanocomposites. A broad band occurred at 1620 cm^{-1} is attributed to bending vibration of H−O−H. The peaks centered at 525, 681, and 982 cm^{-1} are due to the υ(V−S−V) doubly bounded S^{2-}, doubly bridged S^{2-} and υ(V═S) terminal S stretches in the composites, respectively.[27,48] The slightly reduced peak intensity of VS_2/GNS composites, and the appearance of peak vibrations at 1407 and 1250 cm^{-1} which are attributed to the stretching of C═C and C−C in graphene,

DOI: 10.1021/acsami.5b03124
ACS Appl. Mater. Interfaces 2015, 7, 13044−13052

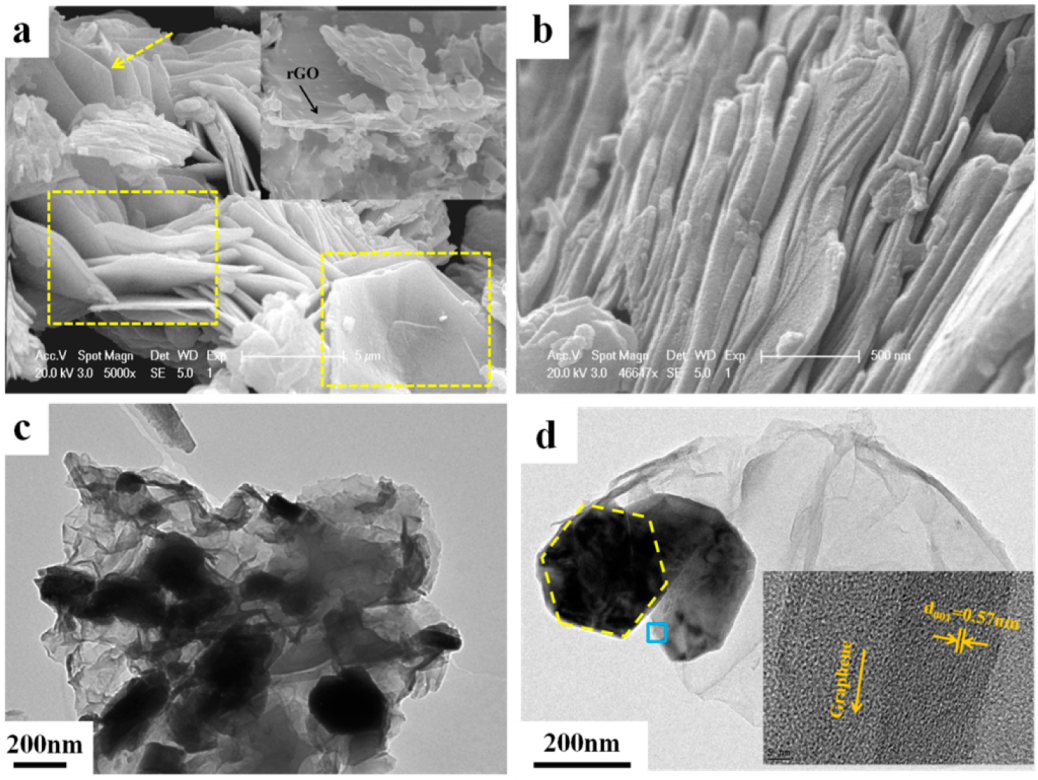

Figure 3. SEM images of (a) VS_2/GNS and (b) pure VS_2; (a, inset) low-magnification of SEM image; (c) TEM and (d) high-magnification TEM images of VS_2/GNS composites; (d, inset) HRTEM image of the area indicated by the blue square in image d.

suggested that VS_2 layers were anchored on graphene sheets in the nanocomposites.

To investigate the morphology and crystallographic features of the VS_2 nanosheets and its graphene composites, we performed SEM, TEM, and HRTEM measurements (Figure 3). SEM and TEM images confirmed that the composites consist of inerratic rGO-attached VS_2 nanosheets, which are slightly stacked together, with sizes range of 50−90 nm in thickness (Figure 3a), naturally as previously expected from our controlled synthesis strategy depicted in Figure 1. Also as shown in Figure 3a,b, obviously layered structure can be observed from the SEM images of VS_2 and VS_2/GNS composites. The thickness of VS_2/GNS nanosheets is almost one-fifth or one quarter that of pure VS_2. Meanwhile, VS_2 nanosheets in Figure 3a appear to have a uniform size and better distribution to a certain bending direction resulting from layer-by-layer growth. In this situation, the enlargement of intersheets gaps caused by the bending growth is beyond our expectation, which will avail a deeper and further research of properties and applications on this material. TEM images in Figure 3c,d further show that a lot of VS_2 nanosheets are homogeneously dispersed on and intimately combined with the surface of rGO over a large area in the nanocomposites. As a result, VS_2 nanosheets enwrapped by a 2D network of graphene layers can effectively increase the intimate contact among VS_2 nanosheets and rGO, which would further improve the electron conductivity and reaction kinetics of the electrodes. The HRTEM image (Figure 3d, inset) presents an interlayer *d*-spacing of 0.57 nm, corresponding to the c parameter of crystalline hexagonal phase VS_2.

Further compared with SEM images of VS_2 with and without CTAB or rGO shown in Figure 4, pure VS_2 is composed of

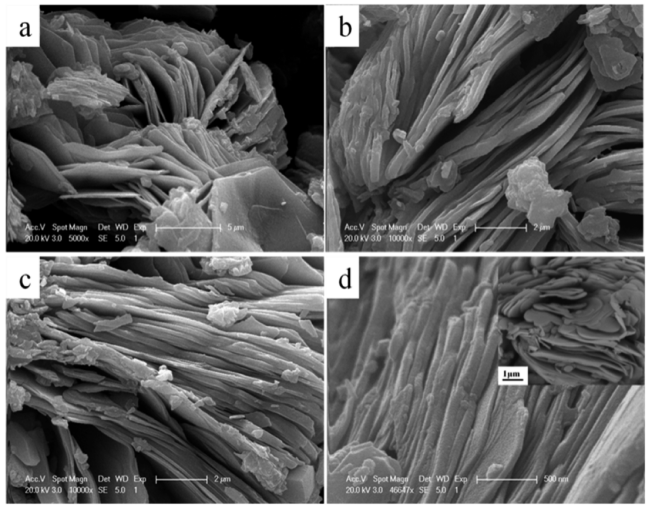

Figure 4. SEM image of (a) VS_2 synthesized with CTAB and rGO, (b) VS_2 synthesized with CTAB, (c) VS_2 synthesized with rGO, (d) pure VS_2, and (d, inset) low-magnification of flower-like nanosheets.

atactic ellipse and tetragon nanosheets with some of which growing together in parallel with flower-shaped morphology (Figure 4d, inset). Moreover, with the addition of CTAB and rGO, VS_2 nanosheets tend to grow into relatively regular hexagonal plates with a sunken center, as shown in Figure 3a,d, denoted districts from an imperfect rudiment with compact stacking, as shown in Figure 4b−d, which is well in accord with the crystal structure. Usually, CTAB as a kind of surfactants is usefull to control crystal morphology in the synthesis of various inorganic nanostructured materials. The comparative results seem to be that CTAB and rGO play a combined role of

DOI: 10.1021/acsami.5b03124
ACS Appl. Mater. Interfaces 2015, 7, 13044−13052

morphology controlling. Absolutely, with sufficient defects as nucleating points, rGO affects the thickness of VS_2 nanosheets. In all, the incorporation of graphene significantly restricts the growth and stacking of VS_2 nanosheets, thus reducing the size of VS_2. Therefore, the presence of agglomeration in TEM image (Figure 3c,d) is believed to be caused by the interaction between VS_2 and rGO.

Further on, Raman spectroscopy was used to characterize the microstructure of the VS_2/GNS composites (Figure 5). In the left region, Raman spectrum of composites exhibits four peaks at 282, 302, 389, and 406 cm^{-1}, which are related to VS_2. The most intensive peak at 282 cm^{-1} corresponding to the E_{1g} mode of hexagonal VS_2 could be caused by a curvature of VS_2 sheets, which is also consistent with the morphology in SEM image.[49] In contrast, in the presence of rGO, the VS_2/GNS composite assembled into flat superposition nanosheets of various sizes (Figure 3b) that perform a slightly weak intensity of counterpart at 282 and 302 cm^{-1}. The drastic morphological difference highlights the important role of rGO as a novel support material for facilitating the nucleation and subsequent growth of nanomaterials. Another two Raman peaks at 389 and 406 cm^{-1} mostly correspond to the in-plane (E_{12g}) displacements of vanadium and out-of-plane (A_{1g}) symmetric displacements of sulfur atoms along the c axis vibration modes.[50] In addition, two distinguishable peaks at about 1351 cm^{-1} (D-band) and 1592 cm^{-1} (G-band) are observed in VS_2/GNS composites in Figure 4b, which confirmed the existence of carbon, as shown in Figure 3a. In general, the G-band is attributed to the vibration of sp^2 carbon atoms with a type of 2D hexagonal lattice, while the D-band is attributed to defects and disorder in the hexagonal graphitic layers.[51] The relative intensity ratio between D and G modes provides information about the degree of the graphene quality. In the present case, the calculated I_D/I_G value of 0.99 agrees well with the presence of rGO, which indicates that the composites contain sp^2 type carbon, thereby enabling good electronic conductivity performance. The broadening and up-shifting of the Raman peaks at 282 and 406 cm^{-1} are particularly significant for the separation of VS_2 sheets, which perhaps attributed to the less-defined stacking structure caused by the interaction between graphene sheets and VS_2 layers.[39,52,53] Therefore, we successfully synthesize morphology controllable of VS_2 and VS_2/GNS composites with the existence of CTAB. Such a thin layered hierarchical structure is expected to provide fast and high electron conductivity based on the excellent contact between VS_2 and graphene, therefore with a potential to improve the dynamic performance of electrode.

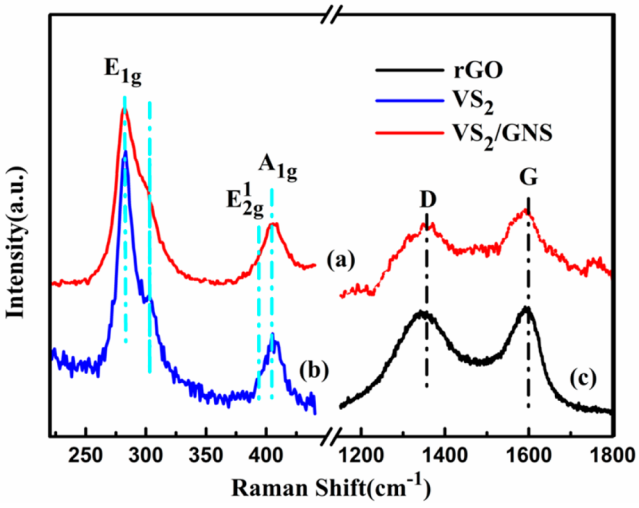

Figure 5. Raman spectrum of (a) VS_2/GNS, (b) pristine VS_2 prepared by hydrothermal route and (c) rGO.

Electrochemical measurements were carried out to evaluate the electrochemical lithiation/delithiation properties of VS_2/GNS nanocomposites as the cathode materials of LIBs. Figure 6 shows CV of the VS_2/GNS nanocomposites at a scan rate of 0.1 mV s^{-1} in the voltage range of 1.5−3.5 V. Similar to VS_2 without rGO, four major pair of cathodic peaks appear in the CV curves of VS_2/GNS electrode at potentials of 2.48, 2.40, 2.33, and 2.20 (vs Li/Li^+), respectively, which can be assigned to possible phase change from α-VS_2 to β-VS_2 during lithium ions intercalating into VS_2 according to $VS_2 + xLi^+ + xe^- \rightarrow Li_xVS_2$.[27] In different stages of discharge process, the VS_2 undergoes series of compositions with x increasing in Li_xVS_2 from the reported partial phase diagram.[30] Interestingly, a pair of remarkable asymmetry peaks appear at the potentials of 2.33 and 2.19 V, denoted with stars, which is most likely related to the concurrent existence of two slightly distorted phase α and β-VS_2. Especially when both d^1 and d^2 vanadium are present, two transitions are frequently observed. In all, the distinguished peaks and the smallest value of potential difference confirmed an enhancement of the electrochemical reversibility and lower ohmic resistance in the electrode reaction. With a special structure and morphology, the cathodic/anodic peak voltages are near, confirming reversible electrochemical reactions between different redox pairs.

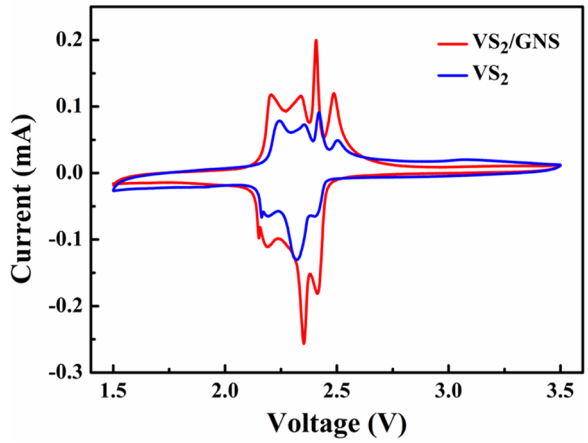

Figure 6. Cyclic voltammograms of the VS_2/GNS nanocomposite electrode at a scan rate of 0.1 mVs^{-1}.

In addition, Figure 7b presents a typical charge/discharge profile of the VS_2/GNS electrode at different current densities in the range of 0.2 to 20 C (1C = 180 mAh g^{-1}). Two plateaus at 2.43 and 2.37 V can be observed at 0.2 C in the first discharge curve, which is correspond well to the two cathodic peaks at 2.48 and 2.40 V, respectively in the CV curve for the first cycle shown in Figure 6. Moreover, with increased charge/discharge current densities, these plateaus become shorter, and plateau voltage difference between charge and discharge increases gradually for the electrode polarization at high current densities. As previously reported,[27,30] these two short plateaus are corresponding with phase transformation between α-VS_2 and β-VS_2 in lithiation/delithiation process. The initial

DOI: 10.1021/acsami.5b03124
ACS Appl. Mater. Interfaces 2015, 7, 13044−13052

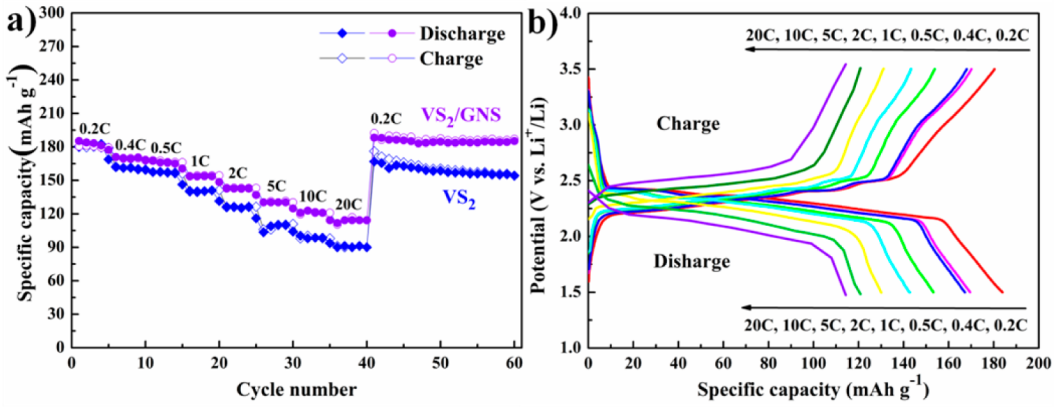

Figure 7. Electrochemical characterization: (a) rate performance of VS_2/GNS nanocomposites and VS_2 and (b) galvanostatic charge−discharge profiles of VS_2/GNS at different current rates.

discharge and charge capacities based on the weight of active material were 185.3 and 180.4 mAh g^{-1}, respectively. Obviously, the incorporation of graphene significantly improves the discharge capacity with 185.3 mAh g^{-1} higher than that of pure VS_2 (Figure 7a) for rechargeable LIBs. To the best of our knowledge, the obtained specific capacity is higher than previously reported.[21,27]

Rate performance is one of the most important characters of electrodes when evaluating the dynamic performance. As seen in Figure 7a, at a high current density of 20 C, the VS_2/GNS electrode still can deliver discharge capacities of 114.2 mAh g^{-1}. However, pristine VS_2 can only reach about 90 mAh g^{-1} at high current density with a succeeding degeneration when cycled at high current density. This result directly suggests a superior rate performance for VS_2/GNS electrode. Furthermore, there is an amazing capacity retention (185.3 → 114.2 mAh g^{-1}) upon the C-rate increase from 0.2 to 20 C and a 99.4% capacity retention after 20 cycles when measured at 0.2 C of the hybrid material. Moreover, when the current density comes back again to 0.2 C, a specific capacity of 188.3 mAh g^{-1} is maintained, which suggests an excellent reversibility and cyclic stability of VS_2/GNS electrode, as previously predicted.[54] It indicates that the structure of VS_2/GNS composite is very stable and retards the aggregation of VS_2 layer during cycles.

The cycling performance was further evaluated at a current density of 0.2 C, as shown in Figure 8. Although some capacity loss upon cycling was observed, the VS_2/GNS electrode exhibited a much slower capacity decay rate than pure VS_2. Pure VS_2 only delivered 113.1 mAh g^{-1} after 200 cycles, corresponding to 63.1% of the initial discharge capacity. In comparison, the VS_2/GNS electrode still maintained a discharge capacity of 160.9 mAh g^{-1}, corresponding to 89.3% of the initial discharge capacity. The good cycling performance could be attributed to the VS_2 sheets supported on the graphene with high conductivity and the layered structure effectively facilitates lithium ion extraction and insertion. The significant architecture of the composite has an indispensible function to protect VS_2 from being pulverized and losing electrical integrity owing to the large volume expansion during discharge/charge cycling.

To obtain deeper electrochemical mechanism in the charging/discharging processes, we performed ex situ XRD measurements (Figure 9). Generally, the XRD patterns remained unchanged except a noticeable change of peak intensity, such as 15.45 and 35.77° during charge/discharge

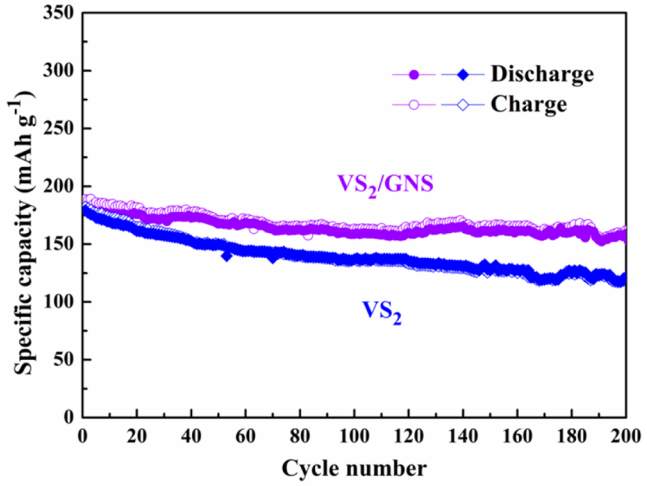

Figure 8. Cycle performance of VS_2/GNS nanocomposites and VS_2 at 0.2 C.

process, as well as the slight change of peak positions, which perhaps characterizes a phase change reaction.[55] In detail, the typical peak intensity of 15.45° increases gradually in the period of Li^+ ion insertion, while the subsequent discharge process appears a counterpart, indicating a completely reversible structure evolution. Interestingly, there is a hysteretic change of peak intensity in the discharge process compared with that in the charge. This can directly contribute to an accumulation of discharge capacity, which is well in agreement with the characterizations of electrochemical test results. Especially, at the end of charge, the peak at 2θ = 15.45° with strong intensity revealed that weak electronic correlation along the *c* axis, and no strong bonding effect is presented between each two neighboring layers. Therefore, a consequence of the microscopic highly c self-orientation of quasi-2D VS_2 nanosheets provides a lower diffusing barrier with an ordered alignment for Li^+ succeeding insertion.[30,56] The peak at 15.2° also slightly moves to higher 2θ during Li extraction and returns to their original values during reinsertion, which is attributed to continuous lattice volume change during cycling. This absolute superiority gives rise to an optimized performance in the presence network of rGO as a matrix to avoid the construction fracture.

To investigate the origin of the enhanced electrochemical performance of the VS_2/GNS nanocomposites, we carried out

DOI: 10.1021/acsami.5b03124
ACS Appl. Mater. Interfaces 2015, 7, 13044−13052

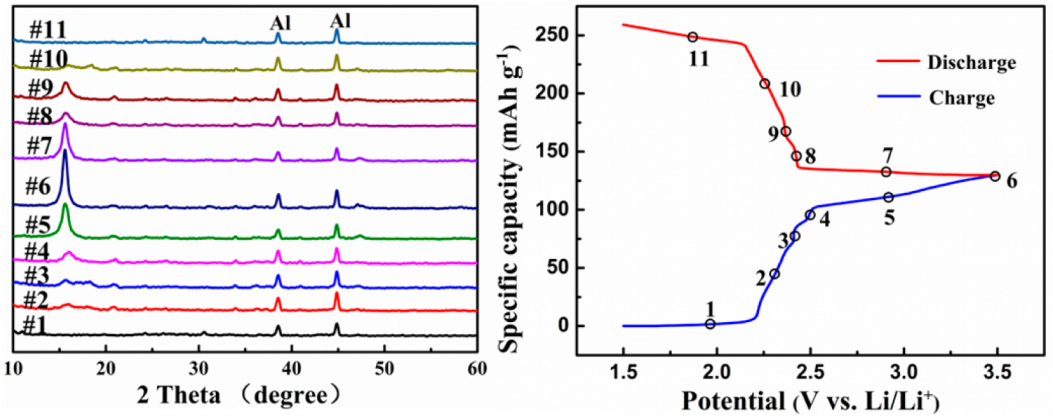

Figure 9. Ex situ XRD spectra of VS_2/GNS electrode obtained at the points denoted in the galvanostatic curve on the right-hand side at 0.2 C.

EIS measurement (Figure 10), which exhibits a semicircle in the high-frequency region and a straight line in the low-frequency region. The semicircle represents the resistance of lithium ion migration through the interface between the surface layer of the particles and the electrolyte, while the straight line indicates the resistance of the diffusion of lithium ions in the bulk of the electrode material. Obviously, the VS_2/GNS electrode has a lower contact and charge transfer resistance than that of the pure VS_2 electrode for its smaller semicircle diameter of 120 Ohm. This result further demonstrates that the incorporation of graphene with VS_2 can effectively enhance the conductivity of rechargeable LIBs, resulting in an improved electrochemical performance. Moreover, the hierarchical structure could effectively prevent structural degradation and delamination of the electrode material from the current collector upon cycling owing to the satisfied rGO matrices, therefore enhancing cycle life and rate performance. In addition, the VS_2/GNS hybrid structure synthesized by controlled nucleation process maximized the synergistic interaction between graphene and VS_2.

To more deeply evaluate the electrochemical behavior of as-synthesized VS_2/GNS composites in a wider potential windows, we test the electrode by galvanostatic charge/discharge in an amplified voltage range from 0.05 to 4 V with a current density of 200 mA g^{-1}. As shown in Figure 11, about 400 mA h g^{-1} of charge capacity is obtained in the initial cycles,

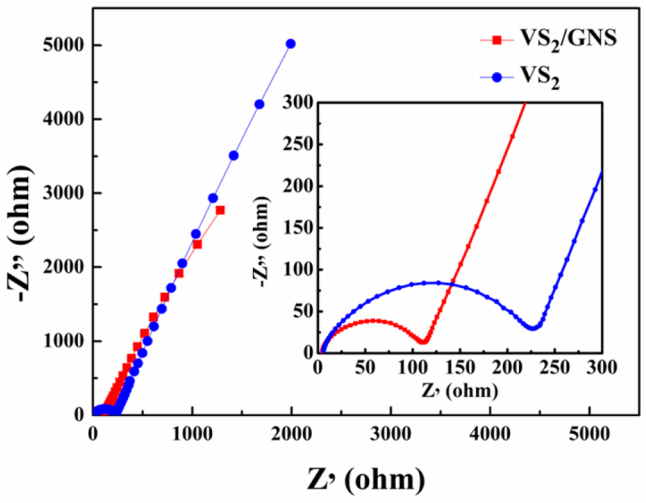

Figure 10. Nyquist plots of VS_2/GNS nanocomposites and VS_2; (inset) enlarged Nyquist plots.

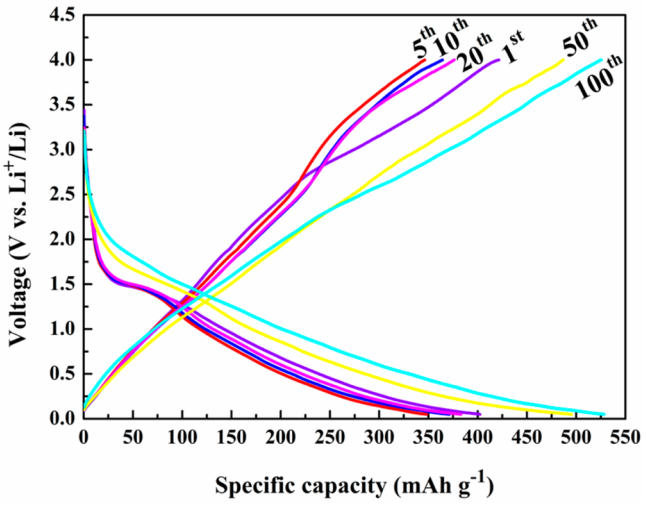

Figure 11. Selected discharge/charge curves at 200 mA g^{-1} of VS_2/GNS composites as anode.

attributing to the synergistic effect between graphene and VS_2, which strengthen their capacity contribution as anode individually. One pair of charge/discharge plateaus occurred at 1.58/1.34 V, which should be attributed to the phase changes of VS_2 in lithiation/delithiation process. The cycling performance (Figure 12) as anode shows a gradual recovery trend until approaching the theory capacity after 40 cycles, indicating an electrochemical activation process of VS_2 and its intermediates.[57] The exact mechanism of electrochemical reaction should be strengthened and investigated in more detail in the future. The excellent electrochemical performance as anode also confirms perfect dynamic performance based on the controlled layered structure, as well as the sufficient contact and synergistic function between VS_2 and graphene.

CONCLUSIONS

In summary, a hierarchical hexagonal architecture VS_2/GNS nanocomposites were successfully fabricated through a simple hydrothermal method in the presence of CTAB for the first time. Various characterizations demonstrate that the layered VS_2 nanosheets are supported on graphene, and its stacking has been significantly inhibited. The VS_2/GNS composites

DOI: 10.1021/acsami.5b03124
ACS Appl. Mater. Interfaces 2015, 7, 13044−13052

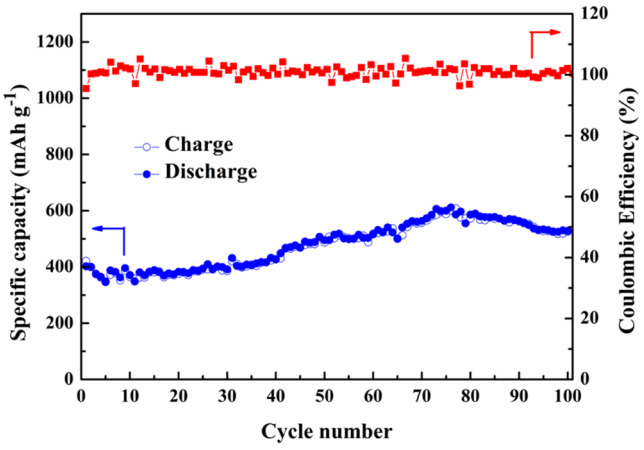

Figure 12. Cycle performance of VS_2/GNS at 200 mA g^{-1} in a voltage range of 0.05−4.0 V as anode.

exhibited a good cycling stability as well as an impressive high-rate capability for lithium storage than pristine VS_2. Even at a high current density of 20 C, the VS_2/GNS nanocomposites still can deliver a discharge capacity of 114.2 mAh g^{-1}, corresponding to 62% of the low-rate capacity. In an expanded electrochemical windows from 0.05 to 4 V, the VS_2/GNS also show a considerable capacity of 525.3 mAh g^{-1} as anode at 200 mA g^{-1} after 100 cycles. Further studies on VS_2 may accelerate the development of transition metal sulfides for LIBs, considering their outstanding performance. With various prerequisites, VS_2/GNS composites may be promising electrode materials for the next generation of rechargeable lithium ion batteries.

AUTHOR INFORMATION

Corresponding Authors

*Tel.: +86 21 66138003. E-mail: hongbinzhao@shu.edu.cn.
*E-mail: zhwchen@uwaterloo.ca.

Notes

The authors declare no competing financial interest.

ACKNOWLEDGMENTS

This work is financially supported by the China Scholarship Council (CSC No. 201406895017), the Shanghai University International Cooperation and Exchange Fund, the Shanghai Education Commission Innovation Project (14YZ016), and the Foundation of State Key Laboratory of Coal Conversion, China (J14-15-603). We also thank the Analysis and Research Center of Shanghai University for sample characterization and the High Performance Computing Center of Shanghai University for structure calculation.

REFERENCES

(1) Song, H.; Lee, K. T.; Kim, M. G.; Nazar, L. F.; Cho, J. Recent Progress in Nanostructured Cathode Materials for Lithium Secondary Batteries. *Adv. Funct. Mater.* **2010**, *20*, 3818−3834.
(2) Armand, M.; Tarascon, J. M. Building Better Batteries. *Nature* **2008**, *451*, 652−657.
(3) Zhang, C. F.; Wu, H. B.; Yuan, C. Z.; Guo, Z. P.; Lou, X. W. Confining Sulfur in Double-Shelled Hollow Carbon Spheres for Lithium−Sulfur Batteries. *Angew. Chem., Int. Ed.* **2012**, *51*, 9592−9595.
(4) Bruce, P. G.; Freunberger, S. A.; Hardwick, L. J.; Tarascon, J. M. Li−O_2 and Li−S Batteries with High Energy Storage. *Nat. Mater.* **2012**, *11*, 19−29.
(5) Liu, N.; Li, W. Y.; Pasta, M.; Cui, Y. Nanomaterials for Electrochemical Energy Storage. *Front. Phys.* **2014**, *9*, 323−350.
(6) Lin, F.; Markus, I. M.; Nordlund, D.; Weng, T. C.; Asta, M. D.; Xin, H. L.; Doeff, M. M. Surface Reconstruction and Chemical Evolution of Stoichiometric Layered Cathode Materials for Lithium-Ion Batteries. *Nat. Commun.* **2014**, *5*, 3529−3537.
(7) Jo, G.; Choe, M.; Lee, S. The Application of Graphene As Electrodes in Electrical and Optical Devices. *Nanotechnology* **2012**, *23*, 1−19.
(8) Edwards, R. S.; Coleman, K. S. Graphene Synthesis: Relationship to Applications. *Nanoscale* **2013**, *5*, 38−51.
(9) Johari, P.; Shenoy, V. Tuning the Electronic Properties of Semiconducting Transition Metal Dichalcogenides by Applying Mechanical Strains. *ACS Nano* **2012**, *6*, 5449−5456.
(10) Eda, G.; Yamaguchi, H.; Voiry, D.; Fujita, T.; Chen, M.; Chhowalla, M. Photoluminescence from Chemically Exfoliated MoS_2. *Nano Lett.* **2011**, *11*, 5111−5116.
(11) Ruben, M. B.; Cristina, G. N.; Julio, G. H.; Felix, Z. 2D Materials: To Graphene and Beyond. *Nanoscale* **2011**, *3*, 20−30.
(12) Xu, M. S.; Liang, T.; Shi, M. M.; Chen, H. Z. Graphene-Like Two-Dimensional Materials. *Chem. Rev.* **2013**, *113*, 3766−3798.
(13) Li, Y. G.; Wang, H. L.; Xie, L. M.; Liang, Y. Y.; Hong, G. S.; Dai, H. J. MoS_2 Nanoparticles Grown on Graphene: An Advanced Catalyst for the Hydrogen Evolution Reaction. *J. Am. Chem. Soc.* **2011**, *133*, 7296−7299.
(14) Wang, Q. H.; Kourosh, K. Z.; Andras, K.; Jonathan, N.; Michael, S. Electronics and Optoelectronics of Two-Dimensional Transition Metal Dichalcogenides. *Nat. Nanotechnol.* **2012**, *7*, 699−712.
(15) Zhu, C. B.; Mu, X. K.; Aken, P. V.; Maier, J.; Yu, Y. Fast Li Storage in MoS_2-Graphene-Carbon Nanotube Nanocomposites: Advantageous Functional Integration of 0D, 1D, and 2D Nanostructures. *Adv. Eng. Mater.* **2015**, DOI: 10.1002/aenm.201401170.
(16) Song, C. Q.; Yu, K.; Yin, H. H.; Fu, H.; Zhang, Z. L.; Zhang, L.; Zhu, Z. Q. Highly Efficient Field Emission Properties of A Novel Layered VS_2/ZnO Nanocomposite and Flexible VS_2 Nanosheet. *J. Mater. Chem. C* **2014**, *2*, 4196−4202.
(17) Choi, S. H.; Kang, Y. C.; Zhang, J. Sodium Ion Storage Properties of WS_2-Decorated Three-Dimensional Reduced Graphene Oxide Microspheres. *Nanoscale* **2015**, *7*, 3965−3970.
(18) Puthussery, J.; Seefeld, S.; Berry, N.; Gibbs, M.; Law, M. Colloidal Iron Pyrite (FeS_2) Nanocrystal Inks for Thin-Film Photovoltaics. *J. Am. Chem. Soc.* **2011**, *133*, 716−719.
(19) Guo, J. X.; Li, F. F.; Sun, Y. F.; Zhang, X.; Tang, L. Graphene-Encapsulated Cobalt Sulfides Nanocages with Excellent Anode Performances for Lithium Ion Batteries. *Electrochim. Acta* **2015**, *167*, 32−38.
(20) Yang, S. L.; Yao, H. B.; Gao, M. G.; Yu, S. H. Monodisperse Cubic Pyrite NiS_2 Dodecahedrons and Microspheres Synthesized by A Solvothermal Process in A Mixed Solvent: Thermal Stability and Magnetic Properties. *CrystEngComm.* **2009**, *11*, 1383−1390.
(21) Rout, C. S.; Kim, B. H.; Xu, X.; Yang, J.; Jeong, H. Y.; Odkhuu, D.; Park, N.; Cho, J.; Shin, H. S. Synthesis and Characterization of Patronite Form of Vanadium Sulfide on Graphitic Layer. *J. Am. Chem. Soc.* **2013**, *135*, 8720−8725.
(22) Chang, K.; Chen, W. X. In Situ Synthesis of MoS_2/Graphene Nanosheet Composites with Extraordinary High Electrochemical Performance for Lithium Ion Batteries. *Chem. Commun.* **2011**, *47*, 4252−4254.
(23) Li, Y.; Wang, H.; Xie, L.; Liang, Y.; Hong, G.; Dai, H. MoS_2 Nanoparticles Grown on Graphene: An Advanced Catalyst for the Hydrogen Evolution Reaction. *J. Am. Chem. Soc.* **2011**, *133*, 7296−7299.
(24) Feng, J.; Peng, L.; Wu, C.; Sun, X.; Hu, S.; Lin, C.; Dai, J.; Yang, J.; Xie, Y. Giant Moisture Responsiveness of VS_2 Ultrathin Nanosheets for Novel Touchless Positioning Interface. *Adv. Mater.* **2012**, *24*, 1969−1974.
(25) Feng, J.; Sun, X.; Wu, C.; Peng, L.; Lin, C.; Hu, S.; Yang, J.; Xie, Y. Metallic Few-Layered VS_2 Ultrathin Nanosheets: High Two-

DOI: 10.1021/acsami.5b03124
ACS Appl. Mater. Interfaces 2015, 7, 13044−13052

Dimensional Conductivity for In-Plane Supercapacitors. *J. Am. Chem. Soc.* **2011**, *133*, 17832−17838.
(26) Therese, H. A.; Rocker, F.; Reiber, A.; Li, J.; Stepputat, M.; Glasser, G.; Kolb, U.; Tremel, W. VS_2 Nanotubes Containing Organic-Amine Templates from the NT-VO_x Precursors and Reversible Copper Intercalation in NT-VS_2. *Angew. Chem., Int. Ed.* **2005**, *44*, 262−265.
(27) Murugan, A. V.; Quintin, M.; Delville, M. H.; Campet, G.; Vijayamohanan, K. Entrapment of Poly(3,4-ethylenedioxythiophene) between VS_2 Layers to Form a New Organic−Inorganic Intercalative Nanocomposite. *J. Mater. Chem.* **2005**, *15*, 902−909.
(28) Ma, Y.; Dai, Y.; Guo, M.; Niu, C.; Zhu, Y.; Huang, B. Evidence of the Existence of Magnetism in Pristine VX_2 Monolayers (X = S, Se) and Their Strain-Induced Tunable Magnetic Properties. *ACS Nano* **2012**, *6*, 1695−1701.
(29) Jing, Y.; Zhou, Z.; Cabrera, C. R.; Chen, Z. F. Metallic VS_2 Monolayer: A Promising 2D Anode Material for Lithium Ion Batteries. *J. Phys. Chem. C* **2013**, *117*, 25409−25413.
(30) Gauzzi, A.; Sellam, A.; Rousse, G.; Klein, Y.; Taverna, D.; Giura, P.; Calandra, M.; Loupias, G. Possible Phase Separation and Weak Location in the Absence of a Charge−Density Wave in Single-Phase 1T-VS_2. *Phys. Rev. B* **2014**, *89*, 235125−235134.
(31) Nethravathi, C.; Rajamathi, M. Chemically Modified Graphene Sheets Produced by the Solvothermal Reduction of Colloidal Dispersion of Graphite Oxide. *Carbon* **2008**, *46*, 1994−1998.
(32) Allen, M. J.; Tung, V. C.; Kaner, R. B. Honeycomb Carbon: A Review of Graphene. *Chem. Rev.* **2009**, *110*, 132−145.
(33) Geim, A. K. Graphene: Status and Prospects. *Science* **2009**, *324*, 1530−1535.
(34) Zhou, G.; Li, F.; Cheng, H. M. Progress in Flexible Lithium Batteries and Future Prospects. *Energy Environ. Sci.* **2014**, *7*, 1307−1338.
(35) Nethravathi, C.; Viswanath, B.; Michael, J. Hydrothermal Synthesis of A Monoclinic VO_2 Nanotube−Graphene Hybrid for Use as Cathode Material in Lithium Ion Batteries. *Carbon* **2012**, *50*, 4839−4846.
(36) Nethavathi, C.; Rajamathi, C. R.; Rajamathi, M.; Gautam, U. K.; Wang, X.; Golberg, D.; Bando, Y. N-Doped Graphene-VO_2(B) Nanosheet-built 3D Flower Hybrid for Lithium Ion Battery. *ACS Appl. Mater. Interfaces* **2013**, *5*, 2708−2714.
(37) Zhao, H. B.; Peng, Z. H.; Wang, W. J.; Chen, X. K.; Fang, J. H.; Xu, J. Q. Reduced Graphene Oxide with Ultrahigh Conductivity as Carbon Coating Layer for High Performance Sulfur@Reduced Graphene Oxide Cathode. *J. Power Sources* **2014**, *245*, 529−536.
(38) Hummers, W. S.; Offeman, R. E. Preparation of Graphitic Oxide. *J. Am. Chem. Soc.* **1958**, *80*, 1339.
(39) Wang, Z.; Chen, T.; Chen, W. X.; Chang, K.; Ma, L.; Huang, G. C.; Chen, D. Y.; Leeb, J. Y. CTAB-assisted Synthesis of Single-layer MoS_2−Graphene Composites as Anode Materials of Li-Ion Batteries. *J. Mater. Chem. A* **2013**, *1*, 2202−2210.
(40) Guo, J. X.; Jiang, B.; Zhang, X.; Liu, H. T. Monodiperse SnO_2 Anchored Reduced Graphene Oxide Nanocomposites as Negative Electrode with High Rate Capacity and Long Cyclability for Lithium-Ion Batteries. *J. Power Sources* **2014**, *262*, 15−22.
(41) Liu, Y. C.; Jiao, L. F.; Wu, Q.; Zhao, Y. P.; Cao, K. Z.; Liu, H. Q.; Wang, Y. J.; Yuan, H. T. Synthesis of rGO-Supported Layered MoS_2 for High-Performance Rechargeable Mg Batteries. *Nanoscale* **2013**, *5*, 9562−9567.
(42) Chang, K.; Chen, W. X. L-Cysteine-Assisted Synthesis of Layered MoS_2/Graphene Composites with Excellent Electrochemical Performances for Lithium Ion Batteries. *ACS Nano* **2011**, *5*, 4720−4728.
(43) Chang, K.; Wang, Z.; Huang, G. C.; Li, H.; Chen, W. X.; Lee, J. Y. Few-Layer SnS_2/Graphene Hybrid with Exceptional Electrochemical Performance as Lithium-Ion Battery Anode. *J. Power Sources* **2012**, *201*, 259−266.
(44) Chang, K.; Chen, W. X. In Situ Synthesis of MoS_2/Graphene Nanosheet Composites with Extraordinarily High Electrochemical Performance for Lithium Ion Batteries. *Chem. Commun.* **2011**, *47*, 4252−4254.
(45) Zhong, M. Z.; Li, Y.; Xia, Q. L.; Meng, X. Q.; Wu, F. M.; Li, J. B. Ferromagnetism in VS_2 Nanostructures: Nanoflowers versus Ultrathin Nanosheets. *Mater. Lett.* **2014**, *124*, 282−285.
(46) Shao, J.; Ding, Y. L.; Li, X. Y.; Wan, Z. M.; Wu, C. Y.; Yang, J. P.; Qu, Q. T.; Zheng, H. H. Low Crystallinity VOOH Hollow Microspheres as an Outstanding High-Rate and Long-Life Cathode for Sodium Ion Batteries. *J. Mater. Chem. A* **2013**, *1*, 12404−12408.
(47) Li, Z. F.; Zhang, H. Y.; Liu, Q.; Liu, Y. D.; Stanciu, L.; Xie, J. Hierarchical Nanocomposites of Vanadium Oxide Thin Film Anchored on Graphene as High-Performance Cathodes in Li-Ion Batteries. *ACS Appl.Mater. Interfaces* **2014**, *10*, 1021−1027.
(48) Liang, B. Y.; Andrews, L. Infrared Spectra and Density Functional Theory Calculation of Group V Transition Metal Sulfides. *J. Phys. Chem. A* **2002**, *106*, 3738−3743.
(49) Koroteev, V. O.; Bulusheva, L. G.; Asanov, I. P.; Shlyakhova, E. V.; Vyalikh, D. V.; Okotrub, A. V. Charge Transfer in the MoS_2/Carbon Nanotube Composite. *J. Phys. Chem. C* **2011**, *115*, 21199−21204.
(50) Sourisseaua, C.; Cavagnata, R.; Fouassiera, M.; Tiradob, J. L.; Moralesb, J. Raman Study and Lattice Dynamics Calculations of Misfit Layered Compounds: $(PbS)_{1.18}TiS_2$ and $(PbS)_{1.12}VS_2$. *J. Mol. Struct.* **1995**, *348*, 107−110.
(51) Xiang, H. F.; Li, Z. D.; Xie, K.; Jiang, J. Z.; Chen, J. J.; Lian, P. C.; Wu, J. S.; Yu, Y.; Wang, H. H. Graphene Sheets as Anode Materials for Li-Ion Batteries: Preparation, Structure, Electrochemical Properties, and Mechanism for Lithium Storage. *RSC Adv.* **2012**, *2*, 6792−6799.
(52) Koroteev, V. O.; Bulusheva, L. G.; Okotrub, A. V.; Yudanov, N. F.; Vyalikh, D. V. Formation of MoS_2 Nanoparticles on the Surface of Reduced Graphite Oxide. *Phys. Status Solidi B* **2011**, *248*, 2740−2743.
(53) Wu, Z. S.; Ren, W.; Xu, L.; Li, F.; Cheng, H. M. Doped Graphene Sheets As Anode Materials with Superhigh Rate and Large Capacity for Lithium Ion Batteries. *ACS Nano* **2011**, *5*, 5463.
(54) Ji, X.; Xu, K.; Chen, C.; Zhang, B.; Wan, H. Z.; Ruan, Y. J.; Miao, L.; Jiang, J. J. Different Charge-Storage Mechanisms in Disulfide Vanadium and Vanadium Carbide Monolayer. *J. Mater. Chem. A* **2015**, *3*, 9909−9914.
(55) Murphy, D. W.; Cros, C.; Disalvo, F. J.; Waszczak, J. V. Preparation and Properties of Li_xVS_2 ($0 \leq x \leq 1$). *Inorg. Chem.* **1977**, *16*, 3027−3031.
(56) Van Laar, B.; Ijdo, D. Preparation, Crystal Structure, and Magnetic Structure of $LiCrS_2$ and $LiVS_2$. *J. Solid State Chem.* **1971**, *3*, 590−595.
(57) Kosidowski, L.; Powell, A. V. Naphthalene Intercalation into Molybdenum Disulfide. *Chem. Commun.* **1998**, *8*, 2201−2202.

DOI: 10.1021/acsami.5b03124
ACS Appl. Mater. Interfaces 2015, 7, 13044−13052